J|A|C|S ARTICLES

Published on Web 02/08/2010

Ultrafast X-ray Solution Scattering Reveals Different Reaction Pathways in the Photolysis of Triruthenium Dodecacarbonyl ($Ru_3(CO)_{12}$) after Ultraviolet and Visible Excitation

Qingyu Kong,*,† Jae Hyuk Lee,‡ Kyung Hwan Kim,‡ Joonghan Kim,‡ Michael Wulff,§ Hyotcherl Ihee,*,‡ and Michel H. J. Koch⊥

Société civile Synchrotron SOLEIL, L'Orme des Merisiers, Saint-Aubin - BP 48, 91192 GIF-sur-Yvette Cedex, France, Center for Time-Resolved Diffraction, Department of Chemistry, Graduate School of Nanoscience and Technology (WCU), KAIST, Daejeon 305-701, Republic of Korea, European Synchrotron Radiation Facility, 6 Rue Jules Horowitz, BP220, F-38043 Grenoble Cedex, France, and European Molecular Biology Laboratory, Hamburg Outstation, EMBL c/o DESY, Notkestrasse 85, D-22603 Hamburg, Germany

Received November 17, 2009; E-mail: kong@synchrotron-soleil.fr; hyotcherl.ihee@kaist.ac.kr

Abstract: Ultrafast (ps) time-resolved X-ray scattering was used to study the structural dynamics of $Ru_3(CO)_{12}$ in cyclohexane after photolysis at 260 nm. Two intermediates form after 100 ps at the onset of the reaction: $Ru_3(CO)_{10}$ for the CO loss channel and $Ru_3(CO)_{11}(\mu$-CO) for the metal−metal cleavage channel. In our previous study at 390 nm, by contrast, three intermediates were observed simultaneously at the onset of the reaction that all relax back to $Ru_3(CO)_{12}$ with different lifetimes. The major difference between photolysis at 260 and 390 nm is that in the first case $Ru_3(CO)_{10}(\mu$-CO) is formed by bimolecular recombination of $Ru_3(CO)_{10}$ with a free CO in 50 ns, whereas in the second case it forms directly from $Ru_3(CO)_{12}$ at the onset of the reaction. The differences between the photofragmentation pathways are related to the absorption bands available at the two wavelengths. The extrema in the difference radial distribution functions (RDFs) are unambiguously assigned by decomposing the total signal into contributions from the solutes, the solvent and the solute−solvent cross-terms, and also contributions from each candidate species. The difference RDFs reveal the depletion of Ru−Ru bonds (2.88 Å) in the initial $Ru_3(CO)_{12}$ molecule and formation of $Ru_3(CO)_{10}$ as the major photoproduct. The high-resolution X-ray (88 keV) scattering pattern of pure liquid C_6H_{12} indicates that the solvent dynamics at early time delays is due to broadening of the intermolecular interatomic correlations at constant volume, whereas during thermal expansion at longer time delays, it results from shifts in these correlations.

Introduction

Several ruthenium complexes play an important role in photocatalysis and photoenergy conversion,[1] but detailed mechanisms for the reactions involved are rarely available, mainly due to the lack of efficient methods to study them. One exception is $Ru_3(CO)_{12}$, a photocatalyst which has served as the paradigm for the photochemistry of transition metal carbonyls. The mechanism of the photolysis of this thermally stable triangular metal carbonyl cluster has been investigated under various conditions by a variety of methods. It has been shown that specific bonds in the complex are broken, depending on the excitation energy (see refs 2, 3 and references therein). In particular, ultrafast infrared spectroscopy revealed that, when solutions of $Ru_3(CO)_{12}$ in noncoordinating solvents such as cyclohexane are excited with either an ultraviolet (266 nm) or a visible (400 nm) optical pulse, competing reactions yield two transient intermediates containing bridging carbonyls, $Ru_3(CO)_{11}(\mu$-CO) (intermediate 1) for the metal−metal cleavage reaction channel and $Ru_3(CO)_{10}(\mu$-CO) (intermediate 2) for the CO loss reaction channel, respectively.[2] This approach is based on monitoring the very specific absorption bands of bridging carbonyls which do not overlap with those of terminal CO groups as illustrated in the IR absorption spectra in Figure 1. In contrast to these highly specific spectroscopic signatures, the signals from X-ray and electron scattering contain contributions from all interatomic distances weighted by the product of the scattering factors of the relevant pair of atoms; that is, all reaction pathways contribute to the scattered signal in proportion to their population and scattering function.[4–15] This makes it, in principle, possible to identify all intermediates at least in the case of simple systems. Ultrafast X-ray solution scattering has been shown to give information that is generally difficult to extract from ultrafast optical spectroscopy such as the time course of changes in bond lengths and angles, including those of short-lived intermediates, on a time scale of picoseconds to milliseconds.[4–7,9–15] Following this approach our recent time-resolved X-ray solution scattering study on $Ru_3(CO)_{12}$ in cyclohexane excited at 390 nm revealed that, beside intermedi-

† Société civile Synchrotron SOLEIL.
‡ Graduate School of Nanoscience and Technology (WCU), KAIST.
§ European Synchrotron Radiation Facility.
⊥ European Molecular Biology Laboratory, Hamburg Outstation.

(1) Tributsch, H. *Coord. Chem. Rev.* **2004**, *248*, 1511.
(2) Glascoe, E. A.; Kling, M. F.; Shanoski, J. E.; Harris, C. B. *Organometallics* **2006**, *25*, 775.
(3) Kong, Q. Y.; Lee, J. H.; Plech, A.; Wulff, M.; Ihee, H.; Koch, M. H. J. *Angew. Chem., Int. Ed.* **2008**, *47*, 5550.

 10.1021/ja9097548

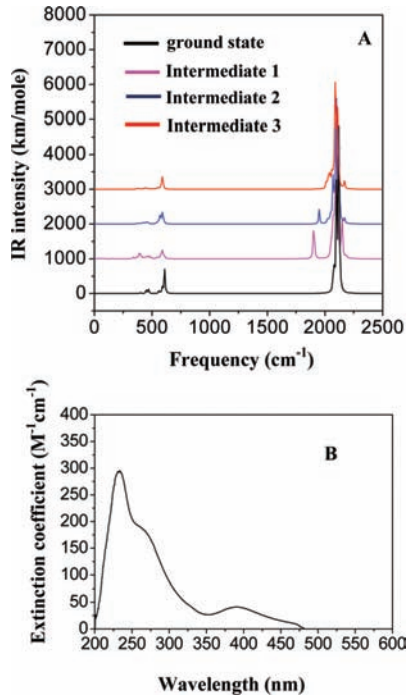

Figure 1. Theoretical IR spectra of the ground state (black), intermediate 1 (magenta), intermediate 2 (blue), and the new intermediate 3 (red) obtained from DFT calculations. (Panel A) Spectra of intermediates 1 and 2 with the characteristic absorption band of the bridging CO groups between 1800 and 2000 cm^{-1}, while there is no absorption band for intermediate 3 in this region. The overlap of the spectra of intermediate 3 and the ground state makes it difficult for time-resolved IR spectroscopy to detect the new intermediate 3 with terminal CO only. (Panel B) UV/visible absorption spectrum of $Ru_3(CO)_{12}$ in cyclohexane.

ates 1 and 2 mentioned above, the major intermediate is actually one of the $Ru_3(CO)_{10}$ isomers with terminal carbonyls only.[3] Ultrafast X-ray absorption spectroscopy (XAS) of metal centers is an alternative technique to study transient molecular species in solution,[16−18] which is highly complementary to ultrafast X-ray scattering. Beside the local structure around the absorbing atoms, which should ideally all have the same or a very limited number of environments, XAS can also give useful information about their oxidation state and coordination numbers.[19] In contrast, the scattering signal contains contributions from all atoms in the system but is rather insensitive to their oxidation state. XAS, of course, also requires that the molecule of interest should contain atoms with experimentally accessible absorption edges.

The UV−vis spectrum of $Ru_3(CO)_{12}$ in cyclohexane has two prominent absorption bands: the first centered at 390 nm and the second peaked at 238 nm with an absorption shoulder at 260 nm as illustrated in Figure 1B. Electronic absorption studies indicate that the lower-energy band at 390 nm originates from the electronic transition $\sigma \rightarrow \sigma^*$ in metal d-orbitals, resulting in heterolytic cleavage of one of the Ru−Ru bonds.[20−22] The short-wavelength absorption band in the UV range has been attributed to metal-to-ligand charge transfer (MLCT) which ultimately results in loss of one carbonyl group in solution.[23,24] As illustrated below, these different absorption processes lead to distinct photofragmentation pathways when $Ru_3(CO)_{12}$ is excited by different wavelengths.

Methods

Experiments. The experimental setup of beamline ID09B at the ESRF has been described elsewhere.[4−7,9−15] Briefly, a 100 fs (fwhm) optical pulse at 260 nm stretched to 2 ps by passing the beam through two 20-cm long SF-10 prisms to lower the peak power and avoid multiphoton absorption was used to excite the $Ru_3(CO)_{12}$ molecules dissolved in cyclohexane. The relaxation of the excited molecules was monitored with a delayed 100 ps (fwhm) X-ray pulse, selected with a synchronized mechanical chopper rotating at a frequency of 986.3 Hz. The scattered X-rays were recorded on a CCD detector with an exposure time of 2 s per image. A time resolution of ~40 ps was achieved by laser time-slicing, i.e. using colinear laser and X-ray beams and scanning the laser pulse position in small steps inside the (longer) X-ray pulse. For time zero, for example, the downstream part of the X-ray pulse becomes a 50 ps long step-truncated Gaussian pulse.[25] An X-ray beam with a 3% bandwidth centered at 17.9 keV (0.69 Å) with 5×10^8 photons per pulse from the single-harmonic U17 undulator was focused into an elliptical $100 \times 60\ \mu m^2$ (fwhm) spot on the sample by a toroidal mirror.

$Ru_3(CO)_{12}$ (99%) (Sigma-Aldrich) and spectroscopic grade cyclohexane (Sigma-Aldrich) (>99.5%) were used without further purification to prepare a ~3 mM solution which was filtered before the measurements. This solution (300 mL) was cycled at 3 m/s through the measurement cell, using a sapphire nozzle producing a 0.3 mm thick liquid sheet.

To follow the kinetics of the transient intermediates, a series of X-ray scattering patterns were collected with an area detector (MarCCD, Mar USA, Evanston, IL) at time delays of −3 ns, −100 ps, 20 ps, 50 ps, 100 ps, 300 ps, 1 ns, 3 ns, 10 ns, 30 ns, 50 ns, 100 ns, 300 ns, 500 ns, and 1 μs relative to the center of the laser

(4) Plech, A.; Wulff, M.; Bratos, S.; Mirloup, F.; Vuilleumier, R.; Schotte, F.; Anfinrud, P. A. *Phys. Rev. Lett.* **2004**, *92*, 125505.
(5) Ihee, H.; Lorenc, M.; Kim, T. K.; Kong, Q. Y.; Cammarata, M.; Lee, J. H.; Bratos, S.; Wulff, M. *Science* **2005**, *309*, 1223.
(6) Kim, T. K.; Lorenc, M.; Lee, J. H.; Lo Russo, M.; Kim, J.; Cammarata, M.; Kong, Q. Y.; Noel, S.; Plech, A.; Wulff, M.; Ihee, H. *Proc. Natl. Acad. Sci. U.S.A.* **2006**, *103*, 9410.
(7) Kong, Q. Y.; Wulff, M.; Lee, J. H.; Bratos, S.; Ihee, H. *J. Am. Chem. Soc.* **2007**, *129*, 13584.
(8) Ihee, H.; Lobastov, V. A.; Gomez, U. M.; Goodson, B. M.; Srinivasan, R.; Ruan, C. Y.; Zewail, A. H. *Science* **2001**, *291*, 458.
(9) Davidsson, J.; Poulsen, J.; Cammarata, M.; Georgiou, P.; Wouts, R.; Katona, G.; Jacobson, F.; Plech, A.; Wulff, M.; Nyman, G.; Neutze, R. *Phys. Rev. Lett.* **2005**, *94*, 245503.
(10) Christensen, M.; Haldrup, K.; Bechgaard, K.; Feidenhans'l, R.; Kong, Q. Y.; Cammarata, M.; Lo Russo, M.; Wulff, M.; Harrit, N.; Nielsen, M. M. *J. Am. Chem. Soc.* **2009**, *131*, 502.
(11) Haldrup, K.; Christensen, M.; Cammarata, M.; Kong, Q. Y.; Wulff, M.; Mariager, S. O.; Bechgaard, K.; Feidenhans, R.; Harrit, N.; Nielsen, M. M. *Angew. Chem., Int. Ed.* **2009**, *48*, 4180.
(12) Lee, J. H.; Kim, T. K.; Kim, J.; Kong, Q. Y.; Cammarata, M.; Lorenc, M.; Wulff, M.; Ihee, H. *J. Am. Chem. Soc.* **2008**, *130*, 5834.
(13) Lee, J. H.; Kim, J.; Cammarata, M.; Kong, Q. Y.; Kim, K. H.; Choi, J.; Kim, T. K.; Wulff, M.; Ihee, H. *Angew. Chem., Int. Ed.* **2008**, *47*, 1047.
(14) Kim, T. K.; Lee, J. H.; Wulff, M.; Kong, Q. Y.; Ihee, H. *ChemPhysChem* **2009**, *10*, 1958.
(15) Ihee, H. *Acc. Chem. Res.* **2009**, *42*, 356.
(16) Chergui, M.; Zewail, A. H. *ChemPhysChem* **2009**, *10*, 28.
(17) Bressler, C.; Milne, C.; Pham, V. T.; El Nahhas, A; van der Veen, R.; Gawelda, W.; Johnson, S.; Beaud, P.; Grolimund, D.; Kaiser, M.; Borca, C. N.; Ingold, G.; Abela, R.; Chergui, M. *Science* **2009**, *323*, 489.
(18) van der Veen, R. M.; Milne, C. J.; El Nahhas, A.; Lima, F. A.; Pham, V.-T.; Best, J.; Weinstein, J. A.; Borca, C. N.; Rafael, A.; Bressler, C.; Chergui, M. *Angew. Chem., Int. Ed.* **2009**, *48*, 2711.
(19) Bressler, C.; Chergui, M. *Chem. Rev.* **2004**, *104*, 1781.
(20) Johnson, B. F. G.; Lewis, J.; Twigg, M. V. *J. Organomet. Chem.* **1974**, *67*, C75.
(21) Desrosiers, M. F.; Ford, P. C. *Organometallics* **1982**, *1*, 1715.
(22) Malito, J.; Markiewitz, S.; Poe, A. *Inorg. Chem.* **1982**, *21*, 4335.
(23) Bentsen, J. G.; Wrighton, M. S. *J. Am. Chem. Soc.* **1987**, *109*, 4530.
(24) Graff, J. L.; Sanner, R. D.; Wrighton, M. S. *J. Am. Chem. Soc.* **1979**, *101*, 273.
(25) Neutze, R.; Wouts, R. *J. Synchrotron Rad.* **2000**, *7*, 22.

excitation pulse. To extract the changes from the laser excitation only, difference images were obtained by subtracting the images in absence of the pump from those in the presence of the optical pump. The image at −3 ns was used as reference (absence of pump) in the subtraction, and another negative time delay at −100 ps was used to check the stability of time zero. The difference intensities $\Delta S(q,t)$, obtained by azimuthal integration of the difference images, were amplified at high q by multiplying them by q. The resulting $q\Delta S(q,t)$ patterns were used to calculate difference radial distribution functions $r\Delta R(r,t)$ by Fourier-sine transformation.

The effect of heating on the dynamics of the pure solvent was obtained in a separate time-resolved X-ray scattering measurement by exciting liquid cyclohexane with a near-infrared laser pulse (<130 fs) at 1700 nm with a total energy of 60 μJ from a Topas colinear OPA (Quantronix, East Setauket, NY).

The scattering pattern of pure liquid cyclohexane was measured at 88 keV on the ID15 beamline at the ESRF (see ref 26 and references therein).

DFT Calculations. The geometries and energies relative to the initial molecule of all putative intermediates in the photolysis of $Ru_3(CO)_{12}$ were previously calculated and optimized with density functional theory (DFT), as implemented in the Gaussian 03 program[27] (see Table 1S in the Supporting Information of our previous report[3]). The only difference is that the energy of the excited state is 459.1 kJmol^{-1} (4.75 eV) for excitation at 260 nm against 306.1 kJmol^{-1} (3.17 eV) for excitation at 390 nm.

Molecular Dynamics (MD) Simulations. MD simulations of the solute/solvent term (i.e. the packing of liquid around various solute structures) were made using the MOLDY program[28] as described elsewhere.[4–7] A six-center Lennard-Jones potential was used for cyclohexane as described previously,[29] and the intermolecular all-atom Lennard-Jones potential was employed for the solute molecule with the following values for the depth of the potential well (ε in kJ mol^{-1}) and the equilibrium distance (σ in Å): Ru−Ru: $\varepsilon = 0.105$, $\sigma = 2.940$; C−C: $\varepsilon = 0.758$, $\sigma = 3.861$; O−O: $\varepsilon = 0.731$, $\sigma = 3.083$. All molecules were treated as rigid, and no further refinement was made.

Results and Discussion

Difference Scattering and Difference Radial Distribution Curves. Figure 2 shows the difference scattering signal of $Ru_3(CO)_{12}$ in cyclohexane excited at 260 nm as a function of time along with the least-squares fitting with a theoretical model. As illustrated in Figure 2, the difference signal at −100 ps is zero, confirming the accuracy of time zero. At positive time delays, difference features appear and evolve with time. The total signal $\Delta S(q,t)$ can be expressed as the sum of contributions from the structural change of the solute, the change of the solvation cage caused by solute/solvent interactions, and the bulk solvent response to heating and thermal expansion.[3,7,30,31] To explain the measured signal, the experimental $q\Delta S(q,t)$ curves were fitted with the theoretical difference intensities containing the three contributions. Both global fitting linking the energetics of the theoretical curves at all time delays and a simpler process fitting the data at each time delay separately were applied. Detailed descriptions of the fitting procedure are given in our previous reviews.[14,15]

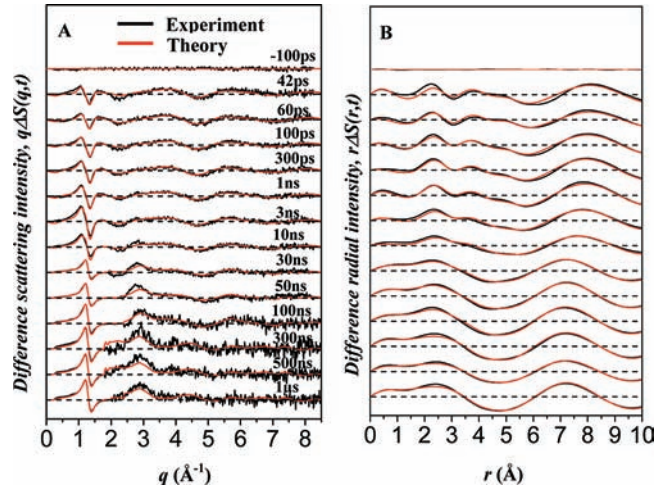

Figure 2. Experimental and theoretical difference scattering intensities, $q\Delta S(q,t)$, and difference radial distributions curves, $r\Delta S(r,t)$. (A) Time-resolved difference scattering intensities $q\Delta S(q,t)$ as a function of time delay after photolysis of $Ru_3(CO)_{12}$ in cyclohexane at 260 nm. The black curves correspond to the experimental data and the red curves to the least-squares fits obtained by fitting the experimental data at each time delay separately. The time delays from top to bottom are −100 ps, 42 ps, 60 ps, 100 ps, 300 ps, 1 ns, 3 ns, 10 ns, 30 ns, 50 ns, 100 ns, 300 ns, 500 ns, and 1 μs. The values in the low q-region of the first six curves and the last seven curves have been divided by 3 and 6, respectively, for better visualization. (B) Difference radial distributions, $r\Delta S(r,t)$, obtained by Fourier-sine transformation of (A).

Although the intensity curves $q\Delta S(q,t)$ in Figure 2A constitute a complete "fingerprint" of the structural rearrangements, the radial real-space RDFS $r\Delta R(r,t)$, obtained by Fourier-sine transformation of $q\Delta S(q,t)$ in Figure 2B, provide a more intuitive picture. The RDF represents the experimental atom−atom pair distribution function during the course of the reaction. It is a measure of the change in radial electron density around an (average) excited atom as a function of interatomic distance r, weighted by the X-ray form factor. As shown in Figure 2B, several positive and negative peaks appear and evolve with time. Peak assignments are, however, complicated due to the three varying components (solute-only, cage, and solvent-only). Unequivocal assignments can only be made by decomposing the signal into its different contributions as illustrated in Figure 3 for the data at 100 ps and 1 μs. From Figure 3B, it becomes clear that the positive peak around 8 Å and the negative peak around 5.6 Å mostly come from the solvent, while the positive peak around 3.7 Å is mostly from the solute−solvent interaction (cage). The solute-only dynamics, which provides the direct information about the molecular structure of the reaction intermediates and reaction mechanism, was obtained by subtracting the contributions of the bulk solvent response and the solvation cage structure in the theoretical model from the measured signals. These differences were then compared with the difference Debye scattering intensities of solutes-only for candidate models. Figure 4 shows such an example at 100 ps. A similar approach has been applied previously.[7] As shown in Figure 4B, the solute-only RDFs display two positive peaks at 2.30 Å, and 5.05 Å and a single negative peak at 3.0 Å. To assign the peaks, the theoretical solute-only difference scattering intensities (red curve in Figure 4) were decomposed into the contributions of intermediates 1, 2, and 3. The difference scattering intensity of each intermediate was calculated from the difference Debye scattering according to its population determined by the least-squares refinement. Figure 4 clearly

(26) Di Michiel, M.; Merino, J. M.; Fernandez-Carreiras, D.; Buslaps, T.; Honkimäki, V.; Falus, P.; Martins, T; Svensson, O. *Rev. Sci. Instrum.* **2005**, *76*, 043702.
(27) Frisch, M. J.; et al. *Gaussian 03*, revision C.02; Gaussian, Inc.: Wallingford, CT, 2004.
(28) Refson, K. *Comput. Phys. Commun.* **2000**, *126*, 310.
(29) Hoheisel, C.; Wurflinger, A. *J. Chem. Phys.* **1989**, *91*, 473.
(30) Soper, A.; Luzar, A. *J. Chem. Phys.* **1992**, *97*, 1320.
(31) Kong, Q. Y.; Kim, J. H.; Lorenc, M.; Kim, T. K.; Ihee, H.; Wulff, M. *J. Phys. Chem. A* **2005**, *109*, 10451.

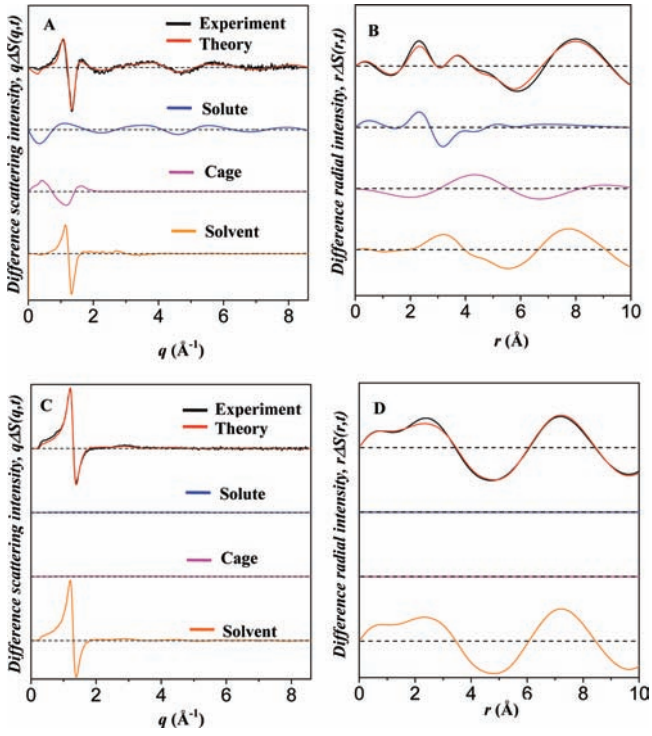

Figure 3. (A) Time-resolved structural reaction dynamics of $Ru_3(CO)_{12}$ in cyclohexane 100 ps after excitation at 260 nm. Contributions to the total theoretical signal (red curve) of the transient solute (blue), solute/solvent interaction (magenta), and the response of the bulk solvent to temperature change (orange). The high q signal can be approximated as originating from naked solutes only, as the cage and solvent signal only significantly contribute at $q < 2$ Å^{-1}. The solute signal is calculated from the Debye scattering of putative solutes, the solute/solvent interaction (cage) from MD simulations, and the solvent signal is deduced from impulsive heating of pure cyclohexane excited with a near-infrared optical pulse. (B) Difference radial intensity $r\Delta S(r,t)$ of $Ru_3(CO)_{12}$ in cyclohexane at 100 ps obtained by sine-Fourier transformation of $q\Delta S(q,t)$ (A). (C) and (D) corresponding structural reaction dynamics of $Ru_3(CO)_{12}$ in cyclohexane at 1 μs. At 1 μs, the intermediate molecules have relaxed to the ground state. The solvent signal dominates at late time delays.

illustrates that the major photoproduct is intermediate 3, while intermediates 1 and 2 have only minor contributions to the total scattering signal. To confirm the fit and give a visual comparison between the difference scattering of each intermediate and the experimental data, the difference Debye scattering of intermediates 1 and 2 were scaled to the same population as for intermediate 3, and the results are superimposed in Figure 4, A and B (dashed curves). Clearly, intermediates 1 and 2 alone cannot fit the experimental data. The decomposed RDFs in Figure 4B indicate that the 2.30 Å peak originates from intermediate 3, which has Ru−Ru distances of 2.66, 2.89, and 2.67 Å (Table 1 in ref 3). The peak positions of these prominent peaks (two positive peaks at 2.30 Å, and 5.05 Å and a single negative peak at 3.0 Å) are displaced from the structural parameters for the initial $Ru_3(CO)_{12}$ molecule and the transient intermediates obtained by time-resolved X-ray scattering (Table 1 in ref 3) due to partial overlap of positive contribution of the intermediate and the negative contribution from the parent molecule. For example, the displacement of the 2.30 Å peak from intermediate 3 results mainly from the overlap of the contributions of the Ru−Ru bond lengths in the transient intermediate and the initial molecule (Ru−Ru = 2.88 Å). The RDFs of intermediate 3 and $Ru_3(CO)_{12}$ in the ground state, as well as their difference curve are shown in Figure 4C. The difference between the Ru−Ru peaks yields a Mexican hat

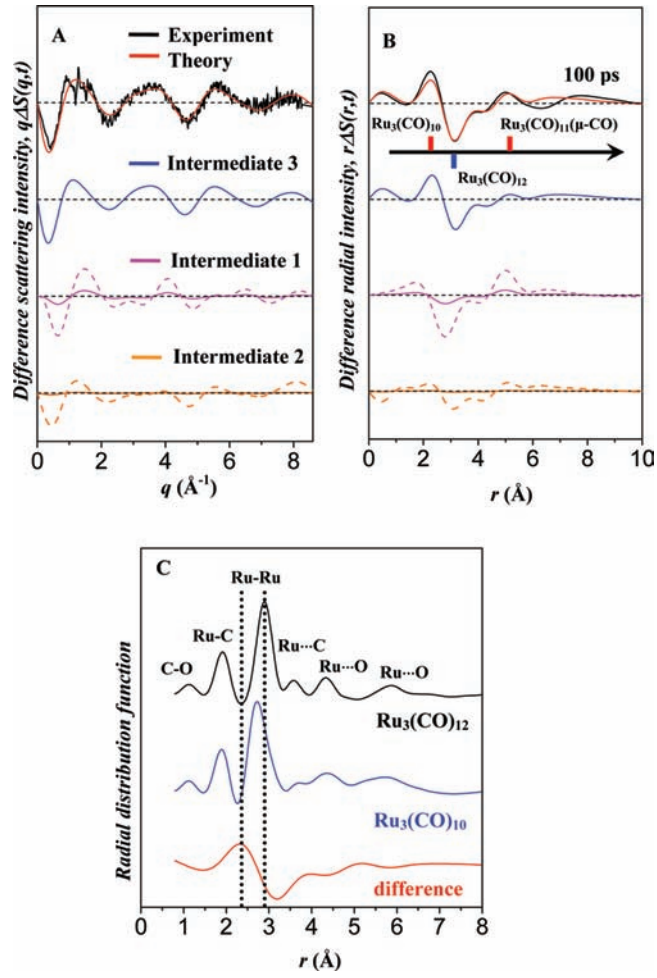

Figure 4. (A) Solute-only experimental (black) and theoretical (red) difference scattering intensities $q\Delta S(q)$ at 100 ps. (B) Solute-only difference radial intensity $r\Delta S(r)$, obtained by Fourier-sine transformation of (A). The solute-only theoretical model (red curve) is decomposed into the contributions from intermediate 3 (blue), intermediate 1 (magenta solid curve), and intermediate 2 (orange solid curve). The difference Debye scattering intensities of each intermediate is calculated using its concentration determined by least-squares fit. The dashed lines represent the difference Debye scattering from intermediates 1 and 2 calculated for the same concentration as for intermediate 3. The decomposition clearly illustrates that intermediate 3 alone can fit the experimental data and is the major photoproduct. (C) The RDFs of $Ru_3(CO)_{12}$ at ground state (black), intermediate 3 (blue), and the difference RDF (red) between intermediate 3 and the ground state. The dashed lines show the positions of the Ru−Ru peaks. It is clear that the Ru−Ru distance in the difference RDF shifts to a shorter distance, producing a "Mexican hat profile". The RDFs of $Ru_3(CO)_{12}$ at ground state and intermediate 3 were obtained by sine-Fourier transformation of the difference between the Debye and the equivalent atomic scattering of each molecule.

profile characteristic of the difference between (partially) overlapping Gaussian profiles where the peak in the difference curve is shifted to shorter distances. Despite the displacement of this peak, the difference RDF clearly reveals the depletion of the Ru−Ru bond in the parent molecule and the formation of the new intermediate 3 which is the major photoproduct.

Reaction Pathways of $Ru_3(CO)_{12}$ in Cyclohexane Excited at 260 and 390 nm. The population changes of various molecular species as a function of time, obtained by global fitting, are shown in Figure 5. Note that intermediates 1, 2, and 3 are shown in black, blue, and red, respectively. With 260 nm excitation (Figure 5B), the dominant $Ru_3(CO)_{10}$ with terminal CO only and $Ru_3(CO)_{11}(\mu$-CO) with metal−metal cleavage are formed

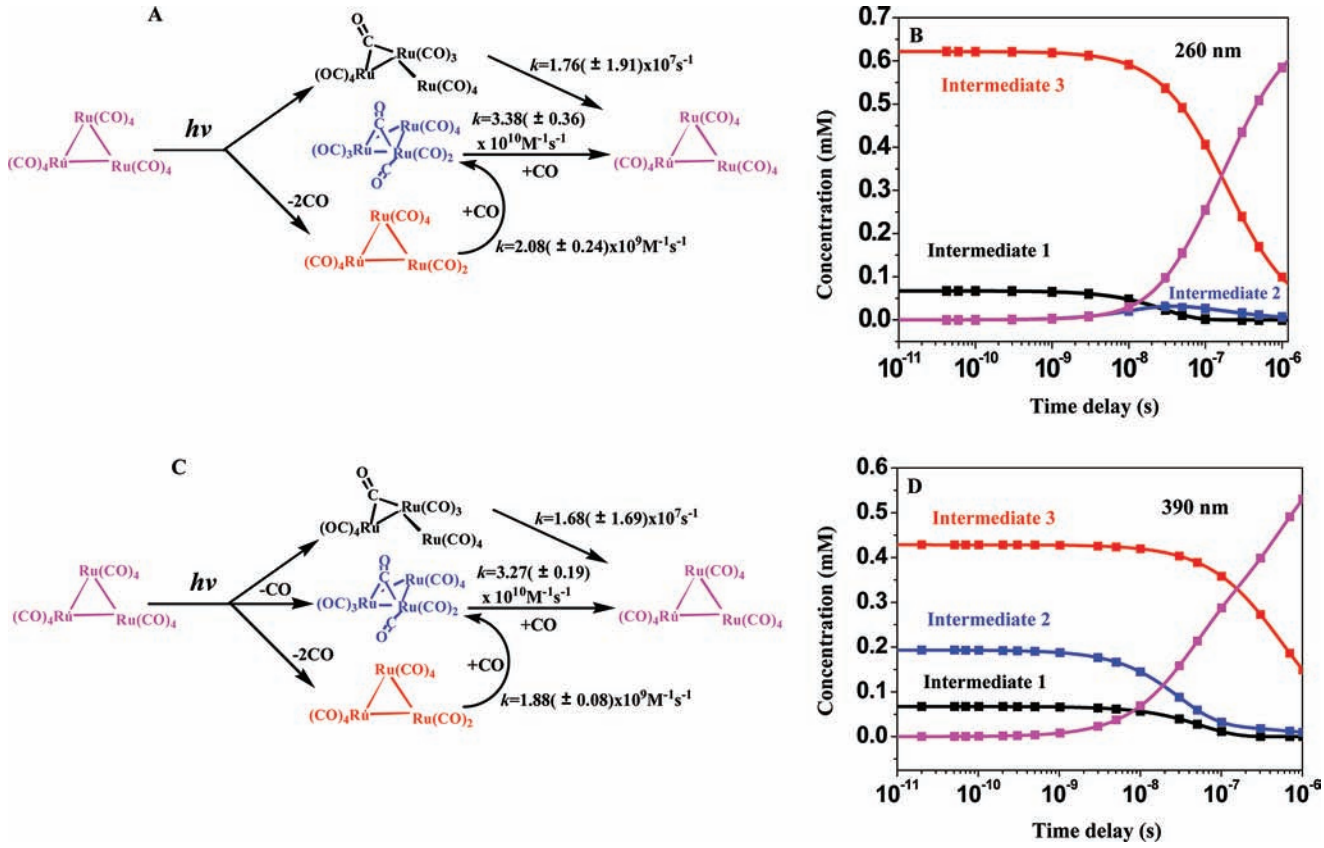

Figure 5. Comparison of the time course of the concentrations changes of intermediates 1 (black), 2 (blue), and 3 (red) during the photoreaction of $Ru_3(CO)_{12}$ and of the rate constants of each reaction channel, after excitation with 260 nm (A and B) with those previously obtained at 390 nm (C and D).[3]

at the onset of the reaction, indicating the rupture of Ru−C and Ru−Ru bonds in $Ru_3(CO)_{12}$ with UV excitation. $Ru_3(CO)_{11}(\mu$-CO) decays exponentially to the initial $Ru_3(CO)_{12}$ with a unimolecular rate constant of 1.76 (±1.91) × 10^7 s^{-1}. Intermediate 2, $Ru_3(CO)_{10}(\mu$-CO), is not formed from the initial molecule at the onset of the reaction, but appears after 50 ns and recombines with a CO ligand to the parent molecule with a bimolecular rate constant of 3.38 (±0.36) × 10^{10} M^{-1} s^{-1}. Intermediate 3 dominates at all time delays. It recombines with a CO ligand to intermediate 2 with a bimolecular rate constant of 2.08 (±0.24) × 10^9 M^{-1} s^{-1}. Since only intermediates 1 and 3 are formed at the onset of the reaction and intermediate 1 decays rapidly to the parent molecule, the only pathway to form intermediate 2 is the recombination of intermediate 3 with one CO. Intermediate 2 does not accumulate as a result of the decay of intermediate 3 (Figure 5B), one possible reason being that intermediate 2 is unstable and rapidly recombines to the initial molecule. The results of the fits indicate that the bimolecular rate constant of intermediate 2 is more than an order of magnitude larger than that of intermediate 3 which explains their population changes. It should be noted that the rate constants observed for the 260 nm excitation are the same as those for 390 nm excitation within experimental errors even if they are not restrained to be the same in the global fitting analysis (Figure 5). This gives confidence in the data analysis and indicates that the global fitting analysis is a stable method. The simultaneous formation of $Ru_2(CO)_9$, $Ru_2(CO)_8$, or $Ru_2(CO)_6$ dimers by loss of one of the monomer units $Ru(CO)_3$, $Ru(CO)_4$,or $Ru(CO)_5$, although thermodynamically favored (Table 1S, in ref 3), is not observed. In a recent theoretical study, the optimized global energy minimum of $Ru_3(CO)_{10}$ corresponds to one of the isomers with bridged CO and C_{3v} symmetry.[32] Inclusion of this $Ru_3(CO)_{10}$ isomer in the data analysis indicates that its contribution to the scattered signal is insignificant.

The large difference in population changes compared to 390 nm excitation (Figure 5, bottom), comes from $Ru_3(CO)_{10}(\mu$-CO) intermediate 2. It is formed simultaneously with intermediates 1 and 3 at the onset of the reaction at 390 nm, through CO loss from the initial $Ru_3(CO)_{12}$.[3] At 260 nm, however, intermediate 2 is not formed from the initial $Ru_3(CO)_{12}$ at the onset of the reaction but by bimolecular recombination of intermediate 3 and a free CO around 50 ns. The different kinetics at 260 and 390 nm mainly arise from the different electronic states involved in the absorption bands of the initial $Ru_3(CO)_{12}$ molecule at UV and visible wavelengths. Theoretical studies of $Ru_3(CO)_{12}$ have shown that excitation at 390 nm populates both the $\sigma\rightarrow\sigma^*$ and MLCT states directly due to overlap of the two bands,[2,23,24] resulting in the simultaneous formation of metal−metal cleavage and CO loss intermediates at the onset of the photofragmentation reaction. However, only the MLCT state associated with the CO loss reaction channel is initially populated upon UV excitation, and the $\sigma\rightarrow\sigma^*$ state for metal−metal cleavage reaction channel is assumed to be populated through internal energy conversion which takes place within a few hundred femtoseconds.[33,34] The different kinetics at 260 nm is assumed to be mainly due to the much higher energies of UV photons (4.75 eV) compared to those of 390 nm (3.17 eV). With UV

(32) Peng, B.; Li, Q. S.; Xie, Y. M.; King, R. B.; Schaefer, H. F., III. *Dalton Trans.* **2008**, 6977.
(33) Desrosiers, M. F.; Wink, D. A.; Trautman, R.; Friedman, A. E.; Ford, P. C. *J. Am. Chem. Soc.* **1986**, *108*, 1917.
(34) Vlcek, A. J. *Coord. Chem. Rev.* **2000**, *200*, 933.

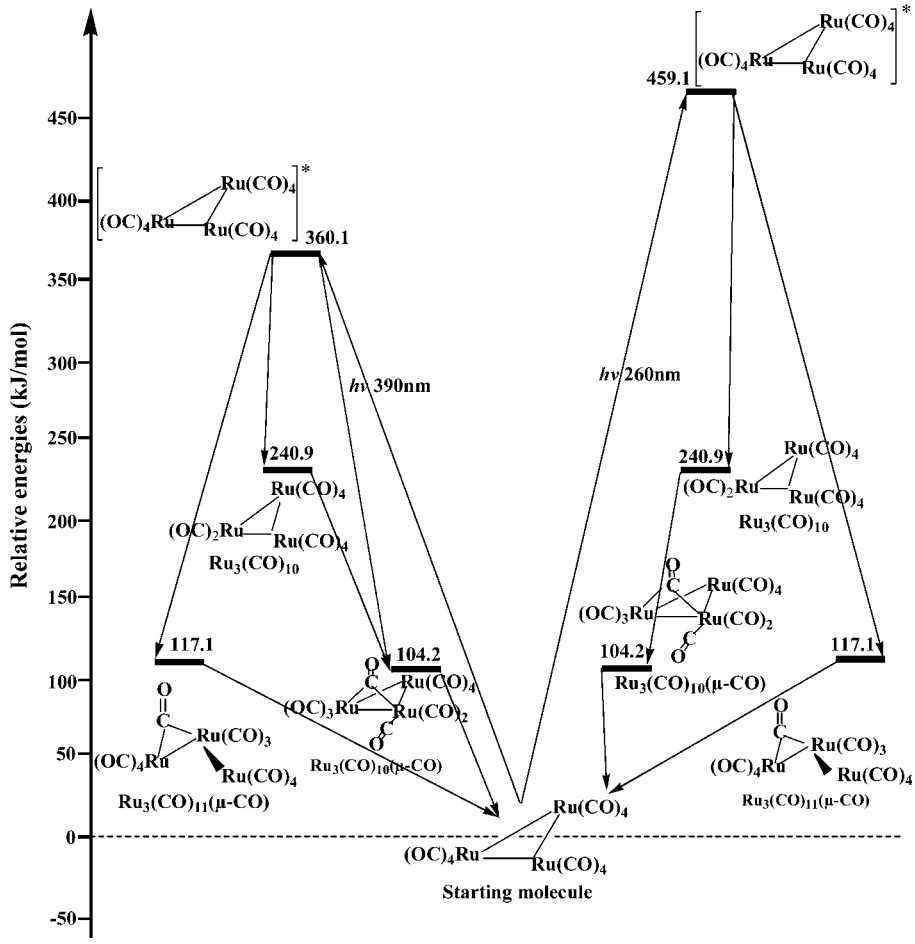

Figure 6. Schematic photofragmentation reaction pathways of $Ru_3(CO)_{12}$ in cyclohexane after excitation at 260 and 390 nm, determined by time-resolved X-ray scattering in solution. With 260 nm excitation, ruptures of Ru−Ru and Ru−C bonds in $Ru_3(CO)_{12}$ lead to $Ru_3(CO)_{11}(\mu$-CO) with bridged CO and $Ru_3(CO)_{10}$ with terminal CO only at the onset of the reaction. The major transient molecule $Ru_3(CO)_{10}$ recombines with one CO ligand to $Ru_3(CO)_{10}(\mu$-CO) which eventually decays into the starting molecule $Ru_3(CO)_{12}$ by recombination with another CO. The $Ru_3(CO)_{10}(\mu$-CO) intermediate is formed through recombination of $Ru_3(CO)_{10}$ during the course of the reaction and does not appear at the onset of the reaction. $Ru_3(CO)_{11}(\mu$-CO) relaxes rapidly to the parent molecule $Ru_3(CO)_{12}$. At 390 nm, three intermediates, $Ru_3(CO)_{11}(\mu$-CO), $Ru_3(CO)_{10}(\mu$-CO) with bridged CO, and $Ru_3(CO)_{10}$ with terminal CO only, are formed at the onset of the reaction from the initial molecule $Ru_3(CO)_{12}$. The subsequent reactions are similar to those at 260 nm. The values show the relative energies in kJ/mol.

excitation a competing dissociation reaction favors the simultaneous loss of two CO, forming $Ru_3(CO)_{10}$ only at the onset. $Ru_3(CO)_{10}$ then recombines nongeminately with a free CO to intermediate 2. The dynamics of the $Ru_3(CO)_{10}$ intermediate 3, which is the major photoproduct and dominates at all time delays as shown in Figure 5, is similar for the two excitation wavelengths. Careful inspection of Figure 5 reveals that with the same initial $Ru_3(CO)_{12}$ concentration, the concentration of intermediate 3 is 45% higher with excitation at 260 nm than with 390 nm. Previous flash photolysis studies on $Ru_3(CO)_{12}$ in cyclohexane indicated that the quantum yields of CO loss intermediates increase significantly as the excitation wavelength is shortened,[35] which is consistent with our observation. The concentration and dynamics of $Ru_3(CO)_{11}(\mu$-CO) with metal−metal cleavage at 260 nm are almost identical to those with 390 nm excitation (Figure 5), which is in agreement with previous conclusions that the photofragmentation quantum yields for metal−metal cleavage reaction channel are wavelength independent.[21,35,36]

In a previous matrix-isolation study at 90 K, it was reported that a transient intermediate $Ru_3(CO)_{11}$ with terminal CO only is formed through loss of one equatorial CO from the starting molecule $Ru_3(CO)_{12}$ upon UV and visible excitation.[23] It then converts to $Ru_3(CO)_{10}(\mu$-CO) intermediate 2 with bridged CO by annealing the matrix at 110 K.[23] The result indicated that $Ru_3(CO)_{10}(\mu$-CO) intermediate 2 is formed by the isomerization of $Ru_3(CO)_{11}$ with terminal CO only. Inclusion of this intermediate in the global fitting indicated that within our time resolution its formation in solution is negligible both at 260 and 390 nm excitation. As the higher stability of $Ru_3(CO)_{10}(\mu$-CO) intermediate 2 (37 kJ mol^{-1}) compared that of to $Ru_3(CO)_{11}$ with terminal CO only (Table 1S in ref 3) provides a thermodynamic driving force for the isomerization reaction,[2] it is likely that this reaction is too fast to be detected with the current time resolution.

The populations of the other intermediates obtained by time-resolved X-ray scattering are less reliable than those obtained from the specific spectroscopic signal especially for minor species such as intermediate 1. As shown previously, a good fit to the 390 nm excitation data can be obtained with intermediates 2 and 3 only.[3] Intermediate 1 was introduced in the analysis mainly for consistency with ultrafast spectroscopy.

(35) Desrosiers, M. F.; Wink, D. A.; Ford, P. C. *Inorg. Chem.* **1985**, *24*, 1.
(36) Grevels, F. W.; Klotzbucher, W. E.; Schrickel, J.; Schaffner, K. *J. Am. Chem. Soc.* **1994**, *116*, 6229.

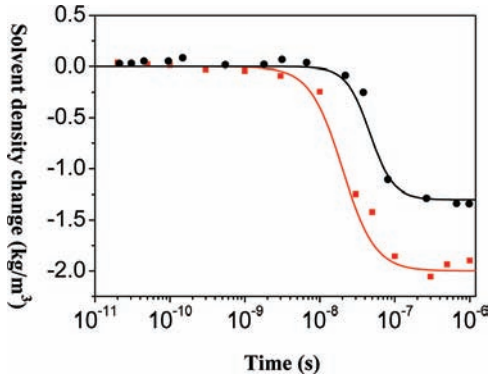

Figure 7. Time course of the change in solvent density ($\Delta\rho(t) = -\lim_{r\to 0}\Delta S(r,t)$) for excitations at 260 nm (red square) and 390 nm (black circle). The scatter curves are Fourier transformed experimental data at $r = 1$ Å from each time delay; the lines are exponential fitting with time scales of 36 ns for 260 nm and 48 ns for 390 nm, respectively.

On the basis of the time dependence of the concentrations of the different intermediates a photodissociation mechanism of $Ru_3(CO)_{12}$ in cyclohexane can be proposed which is compatible with the time-resolved X-ray scattering and ultrafast spectroscopy[2] results: upon excitation at 260 nm, ruptures of the metal−metal and metal−carbon bonds in $Ru_3(CO)_{12}$ lead to simultaneous formation of $Ru_3(CO)_{11}(\mu$-CO) and $Ru_3(CO)_{10}$ at the onset of the reaction. In the course of the reaction the major product $Ru_3(CO)_{10}$ with terminal CO only recombines with a free CO to $Ru_3(CO)_{10}(\mu$-CO), which eventually decays to the starting molecule $Ru_3(CO)_{12}$ by recombination with another CO. At 390 nm, three intermediates, $Ru_3(CO)_{11}(\mu$-CO), $Ru_3(CO)_{10}(\mu$-CO) with bridged CO, and $Ru_3(CO)_{10}$ with terminal CO only, are formed at the onset of the reaction from the initial molecule $Ru_3(CO)_{12}$. The subsequent reactions of $Ru_3(CO)_{10}$ and $Ru_3(CO)_{11}(\mu$-CO) are essentially independent of the excitation wavelength, with $Ru_3(CO)_{11}(\mu$-CO) rapidly relaxing to the parent molecule $Ru_3(CO)_{12}$ through geminate recombination. A schematic photofragmentation pathway is shown in Figure 6. Formation of other species or reaction pathways that occur much faster than the time resolution of our experiments can, of course, not be ruled out. This applies in particular to the possibility that $Ru_3(CO)_{10}$ would be formed from the photofragmentation of some early intermediates.

Structural Dynamics of the Pure Cyclohexane Solvent. As methanol was used as solvent in most of our previous ultrafast X-ray solution scattering,[5–7,12,13] it is useful to consider the structure and dynamics of cyclohexane seen with solution X-ray scattering. As the excited intermediate molecules relax to the ground state, excess energy is released as heat to the surrounding solvent, causing a change of its temperature, pressure, and density. The solvent density change was calculated from the small r limit ($r = 10/q_{max}$) of the radial distribution function as explained previously (ref 3 and references therein). As illustrated in Figure 7, the density change at 1 μs at 260 nm is about 1.5 times larger than that at 390 nm which is consistent with the energy difference of the laser photons at 260 nm (4.75 eV) and 390 nm (3.19 eV).

In general the shifts in the atom−atom distance distributions between solvent molecules are very small, on the mÅ length scale, but given the large molar ratio between solutes and solvent (1:3086 in the present case), the integrated solvent signal can be comparable to or even larger than the solute signal. In the difference X-ray scattering signal the solvent dynamics is usually at low q or high r and dominates at late time delays after the intermediate molecules have relaxed to the ground state (Figure 2). The solvent signal at each time delay can be calculated from the time-dependence of the solvent temperature and density with the following formula:

$$\Delta S_{solvent}(q,t) = \left(\frac{\partial S}{\partial T}\right)_\rho \Delta T(t) + \left(\frac{\partial S}{\partial \rho}\right)_T \Delta\rho(t)$$

where $(\partial S/\partial T)_\rho$ is the change in signal with temperature at constant volume and $(\partial S/\partial\rho)_T$ change in signal with density at constant temperature. These two components were obtained independently with ultrafast X-ray scattering using an infrared laser pulse at 1700 nm to excite the pure solvent and by MD simulations as illustrated in Figure 8, A and B. Figure 8C represents the absorption spectrum of pure cyclohexane.

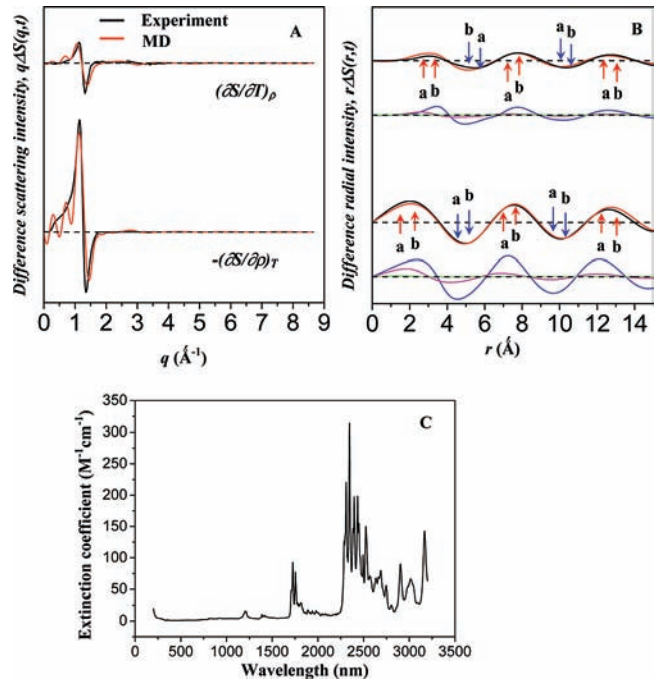

Figure 8. Time-resolved structural dynamics of the cyclohexane solvent. (A) Difference scattering intensity change with temperature at constant volume (top) and the inverse difference intensity change with density at constant temperature (bottom). The black curves are from time-resolved X-ray scattering measurements of pure cyclohexane excited at 1700 nm, while the red curves are from MD simulations. (B) Corresponding radial distribution functions through sine Fourier transformation of (A). RDFs of C···C (blue), C···H (magenta), and H···H (green) from MD simulations are shown below the time-dependent temperature and density curves. The assignments of the main component for major maxima and minima in (B) are given as follows: (a) C···H and (b) C···C. (C) Absorption spectrum of liquid cyclohexane. In the time-resolved X-ray scattering studies on C_6H_{12}, the near-infrared laser pulse at 1700 nm was used for excitation.

Precise assignment of the maxima and minima in Figure 8B requires the X-ray scattering pattern of liquid cyclohexane, which was measured statically with 88 keV X-rays on beamline ID15 at ESRF. Figure 9 shows the difference scattering intensities relative to the equivalent incoherent atomic scattering and the corresponding RDF from top to bottom, respectively. Details about the data analysis of static liquid X-ray scattering can be found elsewhere.[31] The RDF (Figure 9C) reveals both intra- and intermolecular atom−atom distances in pure cyclohexane. The peaks at 1.52, 2.51, and 2.93 Å correspond to the C−C distances between the first, second, and third neighbors of a single C_6H_{12} molecule (see insert C_6H_{12} molecular structure in Figure 9C). The broad oscillation peaked around 6 and 11 Å (insert magnified figure in Figure 9C) is assigned to the

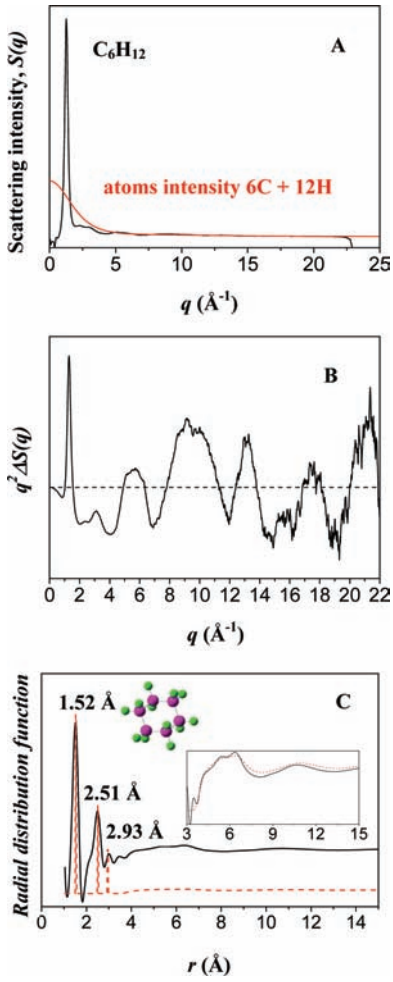

Figure 9. Structure of liquid cyclohexane from high-resolution static scattering at 88 keV. (A) Scattering intensity from C_6H_{12} (black), and the equivalent atomic scattering (red). (B) Difference scattering intensity between the black and red curves in (A), multiplied by q^2 to magnify the signals at high q. (C) RDF of liquid cyclohexane obtained by sine Fourier transformation of (B). The peaks at 1.52, 2.51, and 2.93 Å correspond to the C−C distances between the first, second, and third nearest neighbors inside the C_6H_{12} molecule (inserted cyclohexane molecular structure, C in magenta and H in green). The broad peaks around 6 and 11 Å are assigned to the distribution of C···H and C···C distances in the solvation shells, the intermolecular structure of liquid C_6H_{12} (inserted curves). The red dashed curve shows the RDF of C···C correlations of liquid cyclohexane from MD simulations, for comparison with the experimental curve. The MD signal was scaled to match the experimental curve.

distribution of C···H and C···C distances in the first solvation shell, that is, the C···H and C···C correlations between neighboring C_6H_{12} molecules. This assignment is confirmed by the C−C correlation in the RDF of pure cyclohexane obtained by MD simulations (red dashed curve in Figure 9C).

On the basis of the structural parameters of liquid cyclohexane from static X-ray scattering and MD simulations, the dynamics of C_6H_{12} can be described. At early time delays ($t < 10$ ns), the temperature and pressure of the solvent build up at fixed volume and density. This process is expressed by the first component in the equation and the top curves in Figure 8A and B. The transient thermal response at constant volume, i.e., the positive and negative peaks in Figure 8B (top) are largely due to the broadening of the C···H and C···C correlations between adjacent C_6H_{12} molecules. After about 100 ns, thermal expansion starts and the solvent eventually returns to ambient pressure with a slightly expanded volume, a process described by the second component in the equation and the bottom curves in Figure 8A and B. The peaks and valleys in Figure 8B (bottom) are assigned to shifts in the interatomic C···H and C···C correlations in liquid C_6H_{12}. RDFs of C···C (blue), C···H (magenta), and H···H (green) from MD simulations are shown below the time-dependent temperature and density curves in Figure 8B to clarify the assignment of the peaks and valleys.

Conclusions

Time-resolved X-ray solution scattering on photolysis of $Ru_3(CO)_{12}$ in cyclohexane at 260 and 390 nm reveals three intermediates, $Ru_3(CO)_{10}$ with terminal CO only,[3] $Ru_3(CO)_{11}(\mu$-CO) and $Ru_3(CO)_{10}(\mu$-CO), the latter of which has already been detected by time-resolved infrared spectroscopy.[2] The minor intermediate 1, $Ru_3(CO)_{11}(\mu$-CO), would probably not have been detected by time-resolved X-ray scattering alone, illustrating the fact that ultrafast scattering and spectroscopic methods are indispensable complementary tools in the analysis of reaction mechanisms in solution. Different photodissociation pathways are identified at 260 and 390 nm. Upon UV excitation at 260 nm, at the onset of the reaction, only $Ru_3(CO)_{11}(\mu$-CO) for the metal−metal cleavage channel and the intermediate $Ru_3(CO)_{10}$ with loss of two CO's are formed. In the course of the reaction the major photoproduct $Ru_3(CO)_{10}$ then recombines with a free CO to $Ru_3(CO)_{10}(\mu$-CO), which eventually decays into the starting molecule $Ru_3(CO)_{12}$ by recombination with another CO. After excitation with visible light (390 nm), three intermediates $Ru_3(CO)_{11}(\mu$-CO), $Ru_3(CO)_{10}(\mu$-CO) with bridged CO, and $Ru_3(CO)_{10}$ with terminal CO only are formed from the initial molecule $Ru_3(CO)_{12}$ at the onset of the reaction. The different photofragmentation pathways of $Ru_3(CO)_{12}$ in cyclohexane upon UV excitation presumably originate from the higher photon energy which favors the simultaneous loss of two CO's leading to $Ru_3(CO)_{10}$ only for the CO loss reaction channel at the onset of reaction. The structure and dynamics of the solvent were described at the atomic level, based on the experimental scattering pattern at 88 keV, heating experiments with an infrared laser pulse at 1700 nm, and MD simulations on pure cyclohexane.

Acknowledgment. We thank Rodolphe Vuilleumier and Savo Bratos for their help with the molecular dynamics simulations and theoretical calculations on hydrodynamics of the solvent, Veijo Honkimaki and Thomas Buslaps for their help to measure the static scattering data at 88 keV, and Morten Christensen for measuring the absorption spectrum of pure cyclohexane. This work was supported by Creative Research Initiatives (Center for Time-Resolved Diffraction) of MEST/NRF.

Supporting Information Available: Complete citation of ref 27. This material is available free of charge via the Internet at http://pubs.acs.org.

JA9097548